IPNO DRE 95-18

Role of the breakup process in the ^{48}Ca(^{20}Ne,^{19}Ne n) reaction at 48 A.MeV

H. Laurent[1], J.A. Scarpaci[1], D. Beaumel[1], Y. Blumenfeld[1], S. Fortier[1], N. Frascaria[1], S. Galès[1], J.P. Garron[1], J. Guillot[1], I. Lhenry[1], J.M. Maison[1],J.C. Roynette[1],T. Suomijärvi[1], A. Gillibert[2], P. Roussel-Chomaz[3], and A. Van der Woude[4]

[1]Institut de Physique Nucléaire, IN_2P_3-CNRS, 91406 Orsay Cedex, France
[2]SPhN-DAPNIA, CE Saclay 91191 Gif-sur-Yvette, France
[3]GANIL, BP 5027, 14021 Caen Cedex, France
[4]Kernfysisch Versneller Institut, 9747 AA Groningen, The Netherlands

(July 10, 1995)

Role of the breakup process in the ^{48}Ca(^{20}Ne,^{19}Ne n) reaction at 48 A.MeV

H. Laurent[1], J.A. Scarpaci[1], D. Beaumel[1], Y. Blumenfeld[1] , S. Fortier[1], N. Frascaria[1], S. Galès[1], J.P. Garron[1], J. Guillot[1], I. Lhenry[1], J.C. Roynette[1], J.M. Maison[1], T. Suomijärvi[1], A. Gillibert[2], P. Roussel-Chomaz[3], and A. Van der Woude[4]

[1] *Institut de Physique Nucléaire, IN_2P_3-CNRS, 91406 Orsay Cedex, France*

[2] *SPhN-DAPNIA, CE Saclay 91191 Gif-sur-Yvette, France*

[3] *GANIL, BP 5027, 14021 Caen Cedex, France*

[4] *Kernfysisch Versneller Institut, 9747 AA Groningen, Netherlands*

(July 10, 1995)

Abstract

A study of the reaction ^{48}Ca(^{20}Ne,^{19}Ne n) at 48 A.MeV has been performed at the GANIL facility. The inclusive excitation spectrum above 12 MeV excitation is dominated by a broad structureless bump. Calculations performed in the framework of the Bonaccorso-Brink model predict that the absorption process (transfer+inelastic breakup) dominates over the elastic breakup process. Comparison of the neutron multiplicity calculated in a statistical model with the measured one confirms a significant contribution of the direct processes (elastic and inelastic breakup). The neutron yield to the ground state of the ^{48}Ca is maximal in the forward direction. Comparisons with calculated neutron angular distributions show the effect of the final state interaction.

I. INTRODUCTION

In inclusive spectra of transfer reactions at intermediate energies broad structures appear at high excitation energies embedded in a large structureless background due either to the excitation of non-resonant states or to the contribution of direct processes such as elastic breakup (EBU) or inelastic breakup (IBU). The giant states correspond to excitation of high-spin single particle states far from the Fermi sea [1–3]. The extraction of data on such states is hampered by the underlying background which is usually subtracted empirically. Thus a better understanding of the role played by different processes could make this background subtraction more realistic and might lead to a better understanding of the damping of high-lying excitation in nuclei.

The ^{48}Ca(^{20}Ne,^{19}Ne n) reaction, at 48 A.MeV, has been studied at the GANIL facility. In inclusive experiments, the transfer and the breakup processes cannot be disentangled, but in exclusive experiments, both the measurement of the neutron energy and angular distributions should allow us to distinguish them. Breakup neutrons are expected to be forward peaked in the laboratory frame while the decay neutrons from the transfer reaction exhibit a backward/forward symmetry with respect to the recoil direction. Thus coincidence

measurements with backward emitted particles select the target excitations and correspond to the transfer processes.

Bonaccorso and Brink (B-B) [4,5] have developed a unified model for the one neutron transfer to the continuum in heavy ion reactions. The model treats, in a similar framework, both the absorption into unbound states of the target and the breakup of the projectile in the field of the target nucleus. The difference between the two processes results from the final-state interaction. In the latter case there is no interaction in the final-state. This is the elastic breakup (EBU), or shape elastic breakup in optical model terminology. In the former case, the neutron is absorbed by the target nucleus field. In the B-B model the final-state interaction of the neutron with the target is represented by an optical potential. The absorption can result either in the formation of a compound state (transfer) or in inelastic breakup (IBU) which corresponds to the direct part of the neutron-target optical model absorption. The optical model cannot disentangle the transfer from the IBU in the inclusive cross section calculation while the exclusive experiment does.

However, Bonaccorso and Brink [6] have derived an approximate estimate of the contribution of the IBU to the absorption. They generalize the result obtained for the elastic breakup to the case where the target is excited from the ground state to some final excited state. Assuming that in the final-state interaction, inelastic scattering is a surface effect due mainly to the shape oscillation of the target, they show that the contribution of absorption is limited to a region of space where the surface of the target potential overlaps with the initial state wave function. The complete calculation of the IBU includes the contributions to all the excited states of the target. Nevertheless, they have shown that the sum over all the excited states can be replaced by the imaginary part of the phenomenological optical potential. Using the result of this calculation, the transfer cross section can be extracted from the absorption cross section.

The relative magnitude of the different processes depends strongly on the conditions of the reaction. Single particle state excitations are favoured by the existence of relatively sharp single particle states with appropriate angular momentum matching conditions. On the other hand, the breakup process is favoured by low neutron binding energy in the projectile. In the case of the ^{48}Ca(^{20}Ne,^{19}Ne n) reaction the neutron binding energy is quite large in ^{20}Ne (S_n=16.87 MeV) and the breakup should not be favoured. However, calculations of reference [7] predict that single particle states are relatively weakly excited at 48 A.MeV and are spread over quite a large energy range (figure 1).

II. EXPERIMENTAL SET-UP

The experiment was performed at the GANIL facility by bombarding a 1mg/cm^2 ^{48}Ca target with a 48 A.MeV ^{20}Ne beam. The ^{19}Ne ejectiles were measured in the focal plane of the SPEG spectrometer [9] in coincidence with neutrons detected in the multidetector array EDEN [10]. SPEG was set at 2.5° from the beam and the detected ejectile angles ranged from 0.5° to 4.5°. Unambiguous identification of ^{19}Ne^{10+} was obtained from the $B\rho$, the time of flight and the energy loss measurements. The energy resolution for the ^{19}Ne ejectiles was about 800 keV.

The neutrons were detected in the 40 elements of the multidetector array positioned at 1.75 meters from the target and covering the in-plane angular range [75°→ 160°, -130°→

-150°, -65°→ -95°] and the out-of-plane domain of [-9°→ 9°]. Positive in-plane angles refer to the same side of the beam as the ejectile. In the following, the detectors in the [75°→ 160°] angular range will be referred as "backward detectors" since they are set at angles larger than 90° with respect to the ^{49}Ca recoil direction. The neutron energies were obtained by a time of flight measurement. The liquid scintillator of the EDEN detectors allowed the neutron/gamma-ray pulse shape discrimination.

A Germanium γ-ray detector was set at 55° from the beam and at 25 cm from the target. The efficiency of this detector for 1.33 MeV γ-ray was 80% of a 3"x3" NaI crystal.

III. EXPERIMENTAL RESULTS

Figure 2a displays the ^{49}Ca inclusive spectrum from the ^{48}Ca(^{20}Ne,^{19}Ne) reaction. It is worth noting that for the breakup process the "excitation energy" just means the energy available in the center of mass of the ^{48}Ca+n frame. The detailed analysis of the low excitation energy data being beyond the scope of this paper, only the main features of this part of the excitation energy spectrum are presented. The strong peak (labeled 2) at 4 MeV corresponds to the excitation of the 3.99 MeV ($1f_{5/2}$) and 4.01 MeV ($1g_{9/2}$) states which are strongly excited in the ^{48}Ca(d,p) reaction at 56 MeV [11]. The peak around 6.8 MeV (4) corresponds to the excitation of ($1g_{9/2}$) states [11]. The peak (3) at 5.5 MeV corresponds to the transfer of a ($1d_{3/2}$) neutron from ^{20}Ne to the ($1f_{5/2}$,$1g_{9/2}$) states at 4 MeV in ^{49}Ca. This has been confirmed by the Germanium detector data which exhibit a Doppler broadened and shifted gamma peak corresponding to the 1.30 MeV transition of the 1.54 MeV ($3/2^+$) state to the 0.24 MeV ($5/2^+$) state in ^{19}Ne.

The contribution of the ^{20}Ne ($1d_{3/2}$) orbital to the transfer to the 4 and 6.8 MeV states in ^{49}Ca has been estimated. For the 4 MeV states the comparison of the intensities in the inclusive spectrum of the 4 MeV and 5.5 MeV peaks give a 10±1% contribution. For the 6.8 MeV states the contribution has been extracted from the exclusive data. Final energy spectra are defined as follows: for each coincident event the final energy, E_f, is calculated according to the expression

$$E_f = E_x - E_n \frac{M_{^{48}Ca} + M_n}{M_{^{48}Ca}} - S_n \qquad (1)$$

where E_x is the ^{49}Ca excitation energy, E_n the neutron energy in the ^{49}Ca center of mass frame and S_n the separation energy of the neutron in ^{49}Ca, $M_{^{48}Ca}$ and M_n are the masses of the ^{48}Ca and neutron respectively. The data are corrected for the neutron efficiency. An energy bin around E_f=0 defines the transfer from the ($1s_{1/2}$, $1d_{5/2}$ and $1p_{1/2}$) unresolved orbitals in ^{20}Ne. An energy bin around E_f=1.5 MeV defines the transfer from the ($1d_{3/2}$) orbital in ^{20}Ne. By summing the peak at 6.8 MeV in coincidence with the E_f=0 bin and the 8.3 MeV peak in coincidence with the E_f=1.5 MeV bin, a contribution of 21.7±1% from the ($d_{3/2}$) orbital was obtained. Using the same method we have calculated, in the 8-11 MeV excitation range, the ($d_{3/2}$) contribution which amounts to 24±1% . The peak (6) around 11.4 MeV has not been previously identified.

Above 12 MeV excitation energy in ^{49}Ca the spectrum is dominated by a broad and structureless bump. The shape of this spectrum is reasonably well reproduced (continuous

line) by the Bonaccorso-Brink (B-B) model [7]. The calculated cross section has been normalized to the experimental data in the high excitation energy region. In the 16-30 MeV excitation energy range the calculation underestimates the cross section by about 10 to 15%. The calculation predicts that the reaction is dominated by the absorption process (dashed line).

The figure 2b shows the exclusive spectrum corresponding to the backward detectors and corrected for neutron efficiencies. A broad structure shows up around 20 MeV excitation energy. This is the excitation energy range where the L=5, $1h_{11/2}$, single particle state dominates, according to the results of the B-B calculation (Fig. 1). However, this excitation energy region corresponds to an increase in the mean neutron multiplicity (see section III-B), thus it is more likely that this bump is due to the opening of the two-neutron threshold at about 15.1 MeV excitation energy.

The final energy spectrum (Fig. 3), corresponding to the backward detectors, shows a strong decay component to the ground state. The peak around 5 MeV corresponds to the decay of states in ^{49}Ca to the 3^- states at 4.51 and 5.37 MeV and a 5^- state at 5.73 MeV in ^{48}Ca. The attribution to the 3^- final states is supported by the observation in the Germanium detector of a 673 keV γ-ray corresponding to the transition 4506 keV$\rightarrow$3832 keV(2+) and of a 1538 keV γ-ray corresponding to the transition 5369 keV$\rightarrow$3832 keV(2+) [12]. For the 5^- states the primary transitions are not observed and the attribution is a conjecture based on angular momentum considerations and on the statistical model calculations (see later). For excitations energies higher than the two-neutron emission threshold (S_{2n}=15.09 MeV) and for final energies higher than S_n, E_f is no longer the actual ^{48}Ca final energy since we do not know which one of the two emitted neutrons was detected.

A. Angular Correlations

The neutron angular correlations have been measured in the center of mass of the ^{48}Ca+n frame. The measured angular correlation function corresponding to an excitation energy bin ΔE_x and a final energy bin ΔE_f is:

$$W(\theta_{CM}) = \frac{N_n^{CM}(\theta_{CM})}{N_s\ \Delta\Omega/4\pi} \tag{2}$$

where N_n^{CM} is the measured number of neutrons corrected event by event for the detection efficiency and for the ratio of the cross section in the center of mass to the cross section in the laboratory frame, N_s is the number of single events corresponding to the excitation energy bin ΔE_x and $\Delta\Omega$ the solid angle of the neutron detector(s). Figure 4 shows some examples of angular correlations corresponding to the decay to the ground state of ^{48}Ca for different excitation energy ranges. At low excitation energies, the angular correlations are symmetric with respect to 90° as expected for the decay of resonant states populated by a transfer process. At higher energies, the increase of the cross section at forward angles indicates the contribution of direct processes, e.g. elastic breakup or inelastic breakup. Figure 5 shows some angular correlations at different excitation energies in ^{49}Ca for neutrons corresponding to the "statistical bump" above 7.5 MeV in the final energy spectrum . The angular correlations as expected for statistical decay are almost isotropic except for a slight increase of the cross section at forward angles.

By fitting the correlation function of equation (2) with a Legendre polynomial series the neutron branching ratio (or the mean neutron multiplicity) can be extracted:

$$W(\theta_{CM}) = M_n \sum_i a_i P_i(cos\ \theta_{CM}) \quad (3)$$

where M_n is the neutron multiplicity or the branching ratio in the case of neutron transitions to bound states in ^{48}Ca. Figure 6 shows the neutron branching ratios for the decay to the ^{48}Ca ground state and the excited states around 5 MeV. These branching ratios are calculated using the data from the backward detectors only (diamonds) and correspond to the M_n coefficient defined by Eq. (2) and (3). Figure 6b shows that the greater part of the transition to the 5 MeV group is due to the decay of excited states between 10 and 15 MeV in ^{49}Ca. In figure 6c the branching ratio for the sum of the ground state and the 5 MeV excitation group is plotted. In the figures the histograms represent the result of the statistical model (CASCADE) calculation.

While the branching ratio for $E_f \leq 7.5$ MeV is fairly well reproduced by the calculation up to E_x=18 MeV , at higher energy a non-statistical component shows up. Between 12 and 20 MeV, the ground state branching ratio is in between 18% and 6%, which is much larger than the CASCADE predictions and indicates a quite large direct component. In figure 6 the crosses represent the yield of the ground state transition measured in the detectors set between 71° and 80° with respect to the beam direction and on the opposite side to the ejectile (G4 on Fig. 7). For these forward detectors, the direct component is greater than 10% of the total neutron yield, for excitation energies up to 34 MeV.

In figure 7 are shown the final energy spectra for an excitation energy range between 15 and 40 MeV in ^{49}Ca, corresponding to 4 different detector groups with equal solid angles, the angular positions of which are sketched on the left hand side of the figure. For the G4 group, the closest to the recoil direction, a strong ground state component shows up while the spectra are more isotropic for higher final energy states.

By gating on different final energy bins, excitation energy spectra have been built (Fig. 8). For the forward detectors (G4) , the ground state contribution expands up to about 40 MeV excitation energy (figure 8a) while it is restricted to a few MeV for the backward detectors (G1) (figure 8b). Similar spectra, gated on final-energy bins under the two-neutrons threshold, are shown in figures 8c-f. For the G1 detector,s after the "peak" corresponding to the opening of the channel to the final-energy states under consideration, the cross section is almost negligible. These "peaks" correspond to the emission of statistical low energy neutrons. As for the ground state transition, but to a lesser extent, there is a significant contribution of fast energy neutrons in the G4 detectors. This is shown in Fig. 9 where the ratio of the neutron yield in the G4 group to the one in the backward detectors is plotted versus the neutron energy.

The asymetrical angular behaviour is emphasized in Fig. 10 where the ratio of the counts in the G1 detectors to the counts in the G4 detectors are displayed for two different final-energy ranges in ^{48}Ca. While the ratio for the "statistical" part of the final-energy spectrum stands around 0.7 over the whole excitation energy range, it decreases from 1 to less than 0.1 for the "ground state" transtion. Thus for the ground state transition it appears that the EBU process contributes strongly to the neutron spectra in the forward direction, even at angles as large as 70-80° in the laboratory frame.

The neutron angular distributions have been calculated [8] for the elastic breakup using the plane wave approximation for the final wave function of the neutron (continuous line in figure 11). The diamonds in figure 11 represent the experimental results for the angular distribution of "ground state" neutrons detected in the G4 detectors. These points are calculated according to the expression:

$$Y(\theta^n_{lab})_{exp} = \frac{\Delta N_{gs}}{\Delta\Omega}\frac{1}{N_s} \tag{4}$$

where ΔN_{gs} is the number of "ground state" neutrons detected in coincidence with ^{19}Ne corresponding to a defined excitation energy range in ^{49}Ca and corrected event by event for the detection efficiency. To keep only the contribution of the EBU, the counts in the detectors symetrical to the G4 detectors with respect to 90° have been subtracted. This correction is about 50% for E_x=14 MeV, but only between 15-20% for the higher excitation energies. N_s is the number of singles in the same excitation bite.

The sum of Eq. (4) over the total solid angle is equal to the $\frac{N_{gs}}{N_s}$ ratio. N_{gs} is the number of neutrons emitted in 4π sr. Since the contribution of the absorption process has been removed, N_{gs} is the number of neutrons from the elastic breakup. As the neutron multiplicity for the elastic breakup is one and N_s is proportional to the sum of the elastic breakup cross section and the absorption cross section then

$$\frac{M_{gs}}{M_s} = \frac{\sigma_{EBU}}{\sigma_{incl}}$$

where σ_{EBU} and σ_{incl} are the elastic breakup cross section and the inclusive cross section respectively.

To be consistent with the definition of the experimental angular distribution in equation (4,) the calculated angular distribution has been normalized to the ratio of the calculated EBU cross section over the calculated inclusive cross section:

$$\int Y(\theta^n_{lab})_{EBU} d\Omega = \frac{\sigma_{EBU}}{\sigma_{incl}}$$

The calculated angular distribution is maximal in the beam direction and drops dramatically beyond 20°. The calculated angular distributions are much steeper than the measured ones. In the calculation there is no final-state interaction e.g. no distortion of the neutron wave by the target. That might be an explanation of the discrepancy with the experimental angular distribution.

B. Neutron Multiplicity

The mean neutron multiplicity has been extracted from the fit to angular distributions (equations 2,3), using the backward angles only. If the excitation process was the transfer one, then it would give the actual mean neutron multiplicity. The neutron multiplicity is displayed (crossed bars) in figure 12a for excitation energies up to 50 MeV. On the same figure the multiplicity calculated in the framework of the statistical model using the CASCADE code is displayed. The cascade calculation has been performed using the same distribution

of partial cross section σ_L as calculated in the B-B model. Actually the multiplicity is not very sensitive to the L distribution in the compound nucleus. The large discrepancy between the measured and the calculated values implies that in the inclusive cross section (N_s factor in equation [2]) a large fraction arises from processes for which no corresponding neutron is detected at backward angles (EBU or IBU). In equation (2) N_s is proportional to the inclusive cross section (σ_{incl}) i.e. to the sum of the transfer cross section (σ_{trans}) plus the BU (elastic and inelastic) cross section (σ_{bu}). Thus the measured multiplicity is

$$M_n = \frac{\sigma_n}{\sigma_{incl}}$$

while the one calculated by CASCADE is

$$M_n^c = \frac{\sigma_n}{\sigma_{trans}}.$$

If we assume that the backward neutrons only arise from the transfer process and that the calculated multiplicity corresponds to the actual multiplicity for the transfer, then the ratio of the measured multiplicity to the calculated one is just the ratio of the transfer cross section over the inclusive cross section

$$\frac{M_n}{M_n^c} = \frac{\sigma_{trans}}{\sigma_{incl}}. \tag{5}$$

The ratio on the left hand side of Eq. 5 is plotted on Fig. 12b. The ratio on the right hand side of Eq. 5 can be extracted from the B-B model. The transfer cross section is not calculated directly in the optical model. It is deduced from the difference between the absorption cross section and the IBU cross section calculated as indicated in the references [6,8]. In the approximate calculation of the IBU, the exact sum over the different intermediate-states is replaced by the imaginary part of the optical potential [6]. In Fig. 12b, the two different curves represent two different assumptions. The dashed line is just the ratio of the absorption cross section over the inclusive one, and represents the extreme and unrealistic case of negligible IBU cross section. The solid line corresponds to the transfer cross section as deduced from the calculated IBU cross section. The calculation overestimates the transfer cross section by about 15 to 30%.

IV. CONCLUSION

The ^{48}Ca(^{20}Ne,^{19}Ne n) reaction has been studied at 48 A.MeV. At excitation energies above 12 MeV the inclusive excitation spectrum is dominated by a structureless bump. The B-B model predicts that the absorption is the dominant process and reproduces fairly well the experimental spectrum.

The measured mean neutron multiplicity accounts for about 67% to 45% of the multiplicity calculated within a stastistical model (CASCADE), for excitation energies ranging from 15 MeV to 50 MeV respectively. It implies that only roughly 50% of the inclusive cross section comes from the transfer process. Comparison with the B-B model shows that the model overestimates the contribution of the transfer to the inclusive cross section by about 15 to 30%.

The neutron branching ratios for the $^{49}Ca^{*} \rightarrow ^{48}Ca(GS)$ transitions extracted using the data of the backward detectors and compared to the statistical calculation, indicate a sizable direct component. For the forward neutron detectors this component is even stronger (more than 10% over a wide excitation range). This is another argument for the large contribution of direct process like EBU.

Finally the neutron angular distributions calculated in the B-B model framework for the elastic breakup are much steeper than the experimental ones. It is probably because of the lack of final-state interaction in the calculation of the neutron angular distribution.

V. ACKNOWLEDGEMENTS

We wish to thank Dr A. Bonaccorso for communicating her results before publication and for enlightening discussions. We would also thank Dr J.S. Winfield for a carefull reading of this manuscript.

REFERENCES

[1] S. Gales et al., Phys. Rep. **166**, 127 (1988)
[2] Nguyen Van Giai and Ch. Stoyanov, Phys. Lett. B **272**, 178 (1991)
[3] D.Beaumel et al., Phys. Rev. C **49**, 2444 (1994)
[4] A.Bonaccorso and D.M.Brink, Phys. Rev. C **43**, 299 (1991)
[5] A.Bonaccorso and D.M.Brink, Phys. Rev. C **44**, 1559 (1991)
[6] A.Bonaccorso and D.M.Brink, Phys. Rev. C **46**, 700 (1992)
[7] A.Bonaccorso and D.M.Brink, Phys. Rev. C **51**, 822 (1995)
[8] A. Bonaccorso to be published.
[9] L.Bianchi et al., Nucl. Inst. Meth. **A276**, 568 (1989)
[10] H.Laurent et al., NIM **A326**, 517 (1993)
[11] Y.Uozumi et al., Phys. Rev. C **50**,263 (1994)
[12] Nuclear Data Sheets **68**, 7 (1993)

FIGURES

FIG. 1. Transfer cross section to states of different angular momentum in the ^{48}Ca(^{20}Ne,^{19}Ne)^{49}Ca reaction at 48 A.MeV (reference [7]). The labels in the figure correspond to the transfered orbital angular momentum. For each energy the sum over L is normalized to the unity.

FIG. 2. Excitation spectra in the ^{48}Ca(^{20}Ne,^{19}Ne)^{49}Ca reaction at 48 A.MeV. a) Inclusive spectrum. b) Neutron coincident spectrum corrected for the neutron efficiencies and summed over the backward detectors (see text).

FIG. 3. ^{48}Ca final energy spectrum, corrected for the neutron efficiencies and corresponding to the backward detectors.

FIG. 4. Angular correlations in the frame of the ^{48}Ca+n system for neutron transitions to the $^{48}Ca_{G.S}$.

FIG. 5. Same as figure 4 for final energies $E_f \geq$7.5 MeV.

FIG. 6. Neutron branching ratio. a) to the ground state of ^{48}Ca. b) to excited states around 5 MeV. c) sum a)+b). Diamonds: experimental data from the backward detectors. Crosses: experimental data from forward detectors.

FIG. 7. Final energy spectra for different detector groups. The angular position of the groups are sketched on the left hand side of the figure. The corresponding ^{49}Ca excitation energy range is 15-40 MeV.

FIG. 8. Excitation energy spectra in coincidence with neutrons and gated on different final-energy bins.

FIG. 9. Ratio of neutron yield in G1 detectors to the yield in G4 detectors. a) ^{48}Ca final energy $\geq$ 7.5 MeV. b) ground state transition.

FIG. 10. (Forward detectors)/(backward detectors) neutron yield ratio versus the neutron energies.

FIG. 11. Angular distribution in the laboratory frame for neutron transitions to the ^{48}Ca ground state (see text).

FIG. 12. a) Mean neutron multiplicity versus excitation energy in ^{49}Ca. Continuous line, statistical model prediction. Crosses, experimental results using the data of the backward detectors. b) Crosses: ratio of the measured multiplicity to the multiplicity calculated in the statistical model. The dashed and solid lines are the ratio of the transfer cross section to the inclusive cross section as calculated in the B-B model. The dashed line corresponds to the extreme hypothesis of a transfer cross section equal to the absorption cross section (no IBU). The solid line corresponds to the transfer cross section deduced from the IBU cross section calculated in the B-B model (see text)

Fig 1

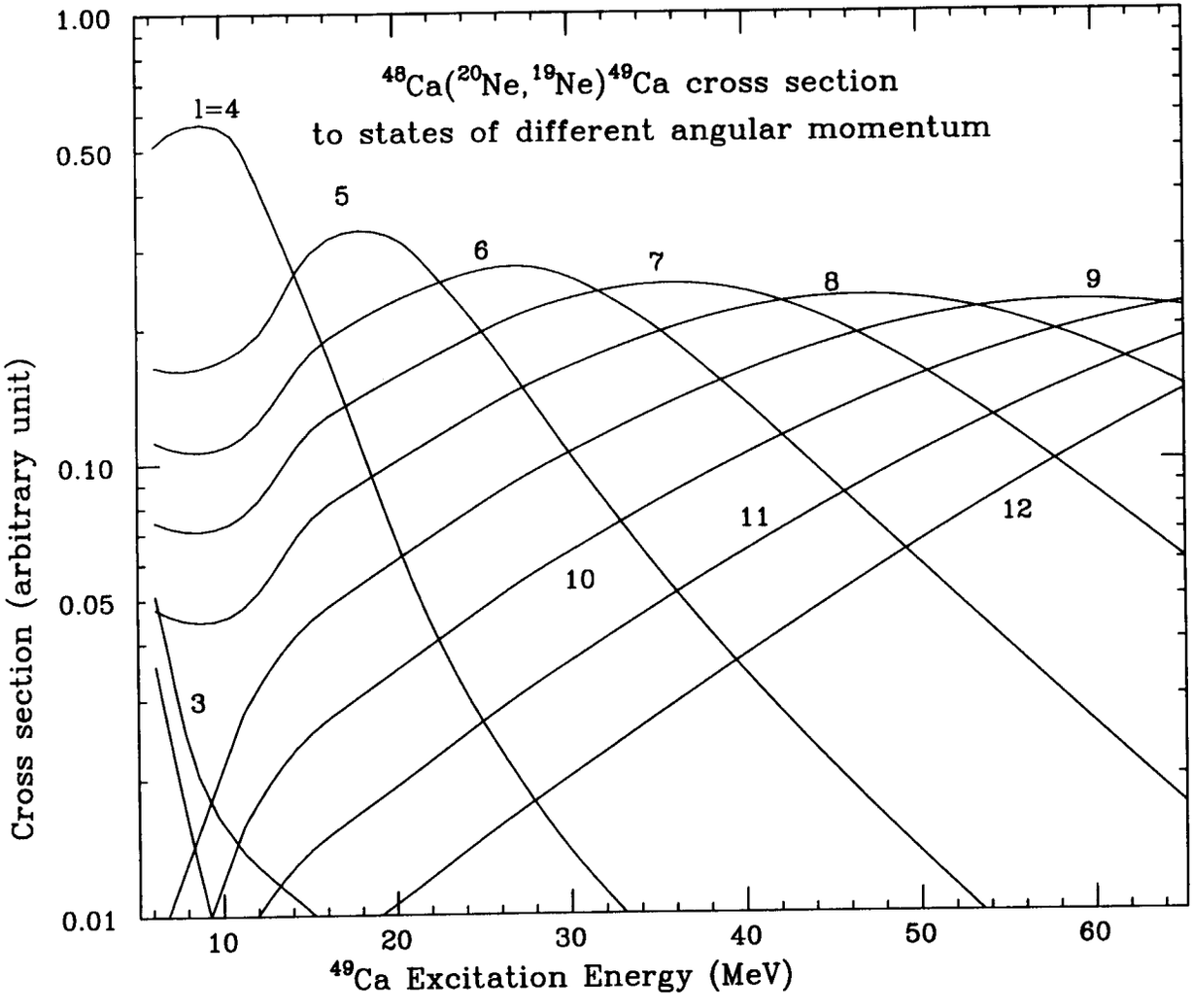
^{48}Ca(^{20}Ne,^{19}Ne)^{49}Ca cross section
to states of different angular momentum
l=4
5
6
7
8
9
10
11
12
3
1.00
0.50
0.10
0.05
0.01
Cross section (arbitrary unit)
10
20
30
40
50
60
^{49}Ca Excitation Energy (MeV)

Fig 2

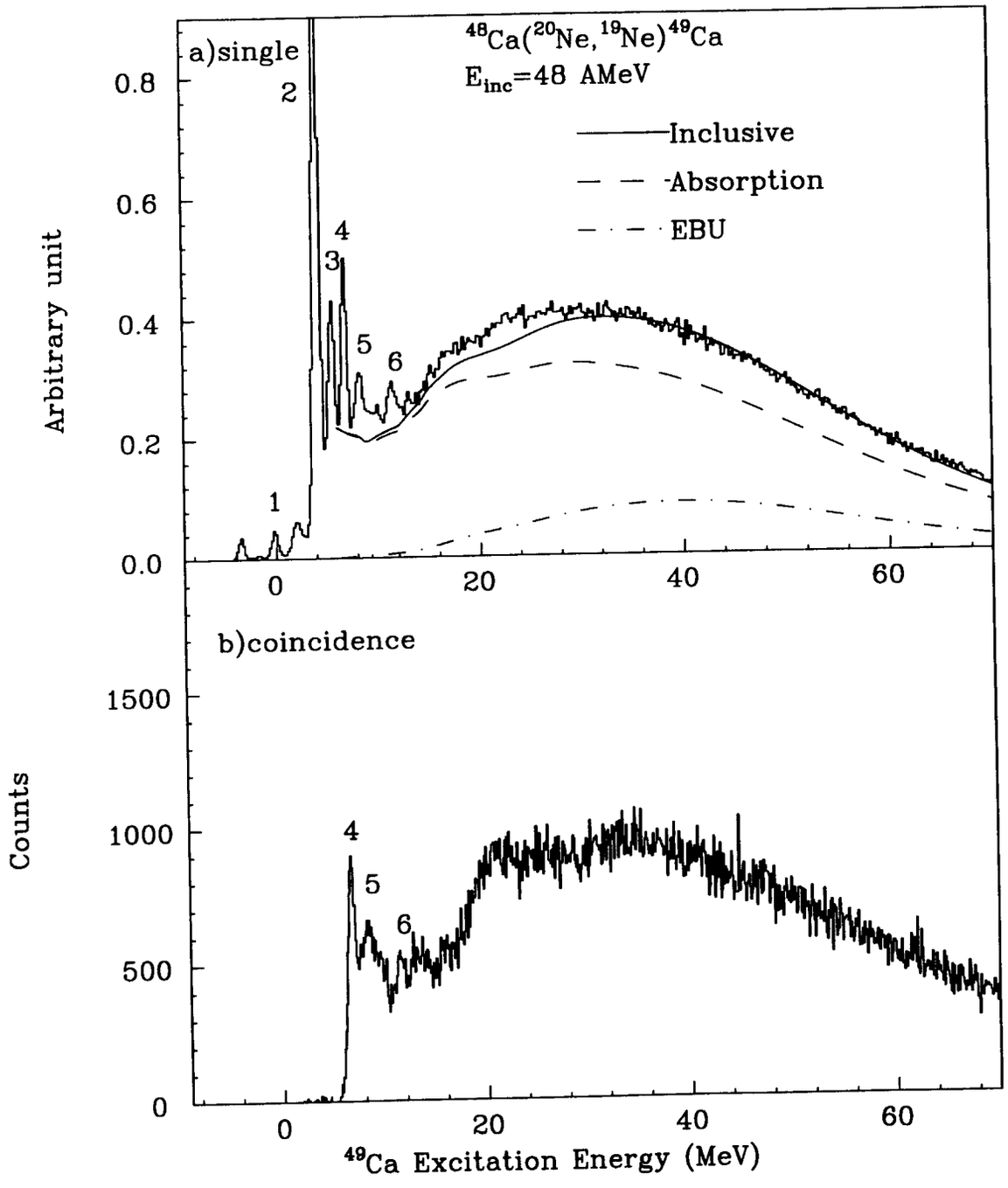
a)single
$^{48}Ca(^{20}Ne,^{19}Ne)^{49}Ca$
E_{inc}=48 AMeV
Inclusive
Absorption
EBU
Arbitrary unit
b)coincidence
Counts
^{49}Ca Excitation Energy (MeV)

Fig 3

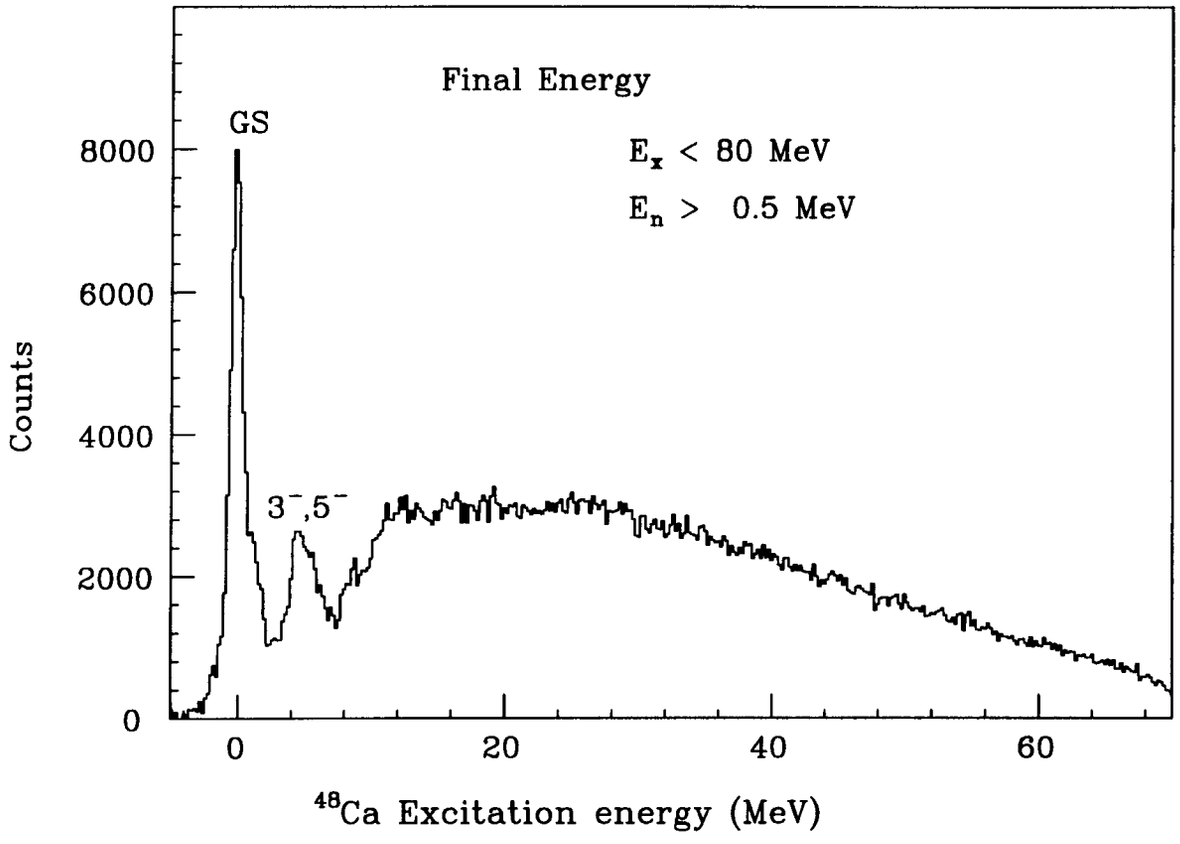
Final Energy
GS
E_x < 80 MeV
E_n > 0.5 MeV
$3^-,5^-$
Counts
8000
6000
4000
2000
0
0
20
40
60
^{48}Ca Excitation energy (MeV)

Fig 4

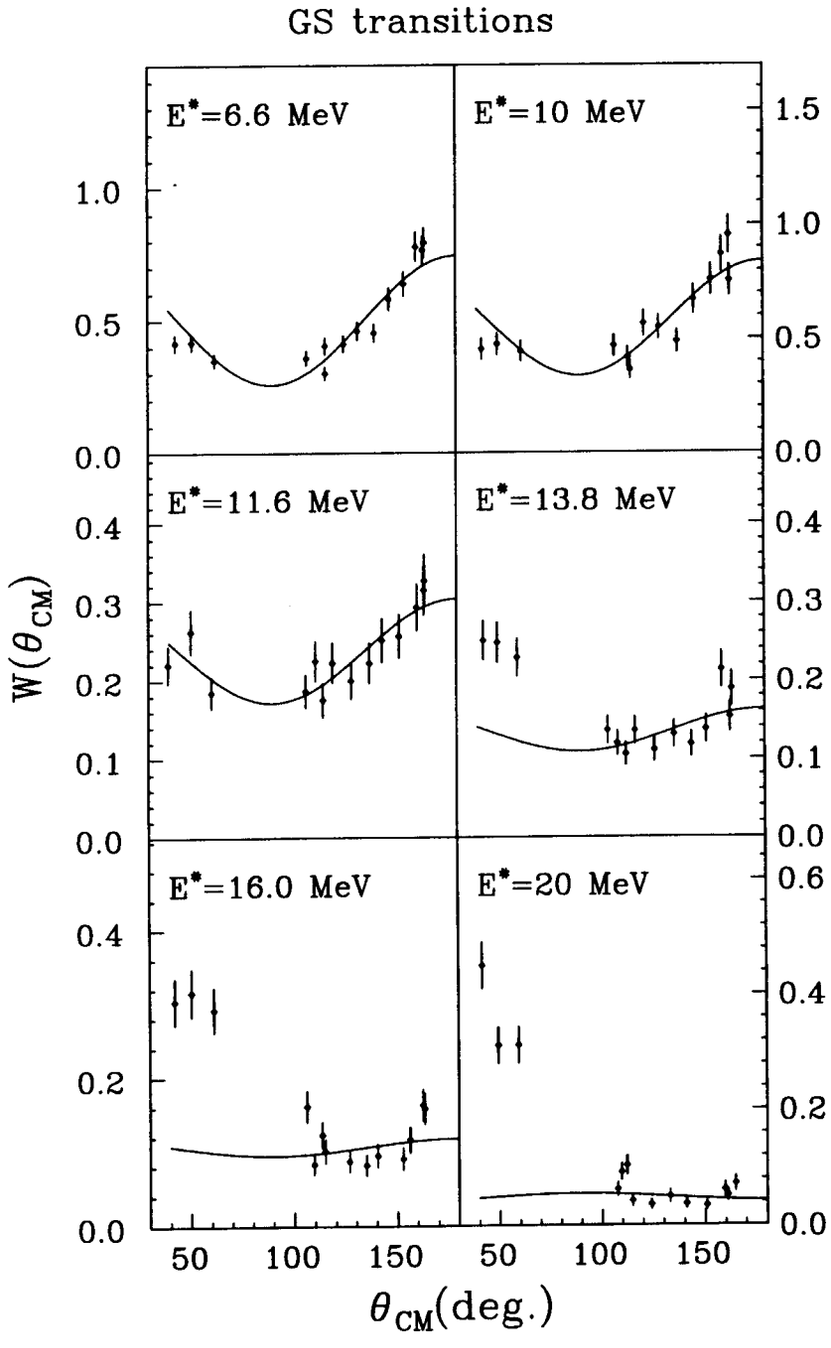
GS transitions
E*=6.6 MeV
E*=10 MeV
E*=11.6 MeV
E*=13.8 MeV
E*=16.0 MeV
E*=20 MeV
W(θCM)
θCM(deg.)
50
100
150

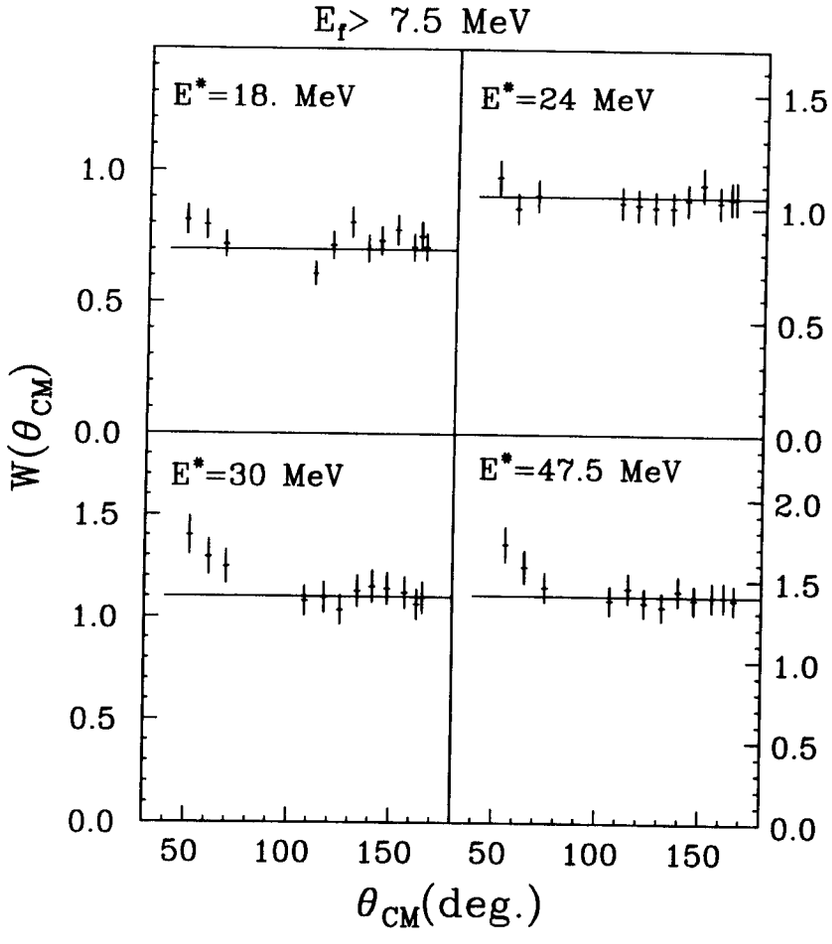
E_f> 7.5 MeV
E*=18. MeV
E*=24 MeV
E*=30 MeV
E*=47.5 MeV
$W(\theta_{CM})$
θ_{CM}(deg.)
0.0
0.5
1.0
1.5
2.0
50
100
150

Fig 6

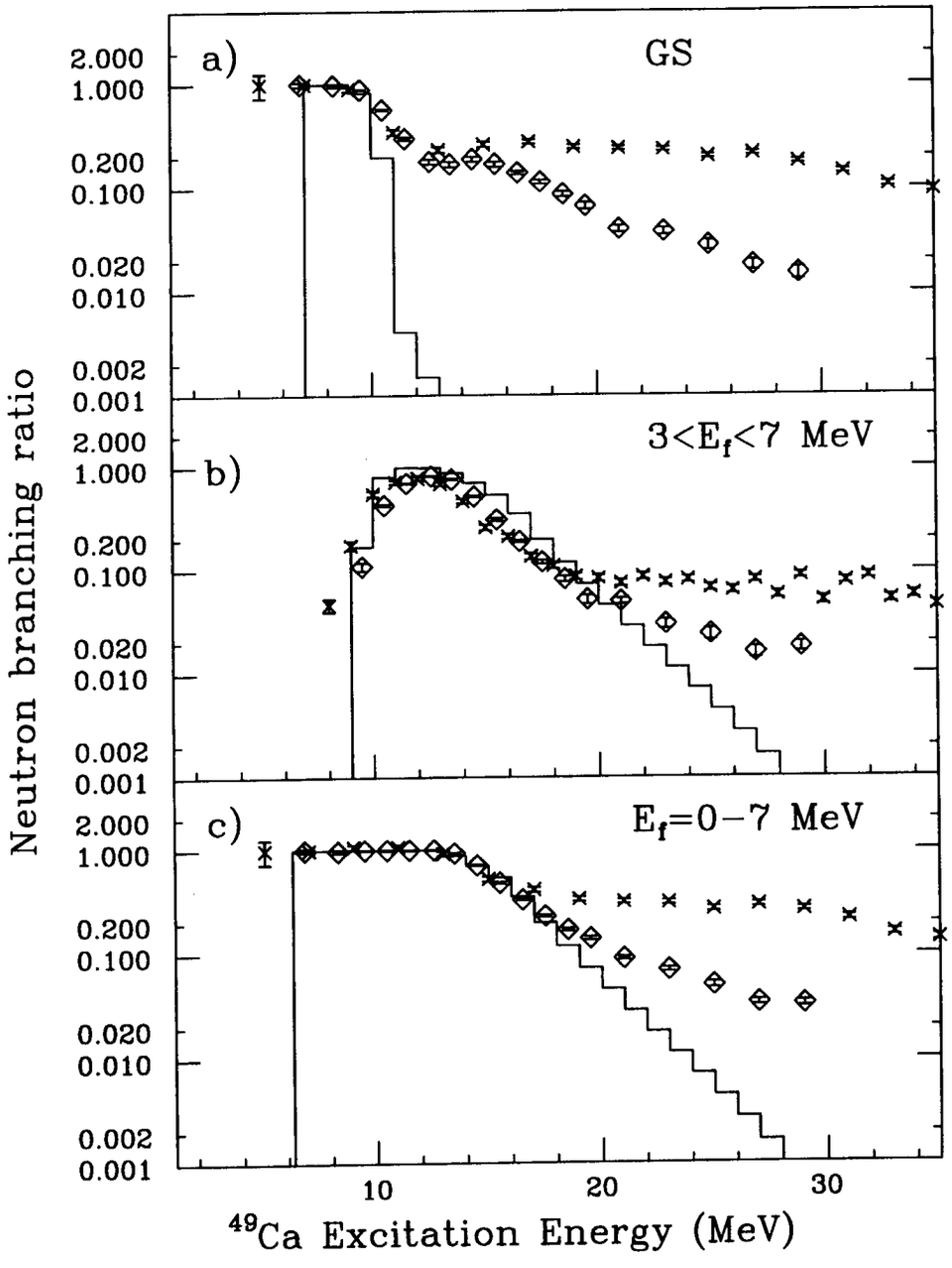
a)
GS
b)
3<E_f<7 MeV
c)
E_f=0−7 MeV
2.000
1.000
0.200
0.100
0.020
0.010
0.002
0.001
Neutron branching ratio
10
20
30
49Ca Excitation Energy (MeV)

fig 7

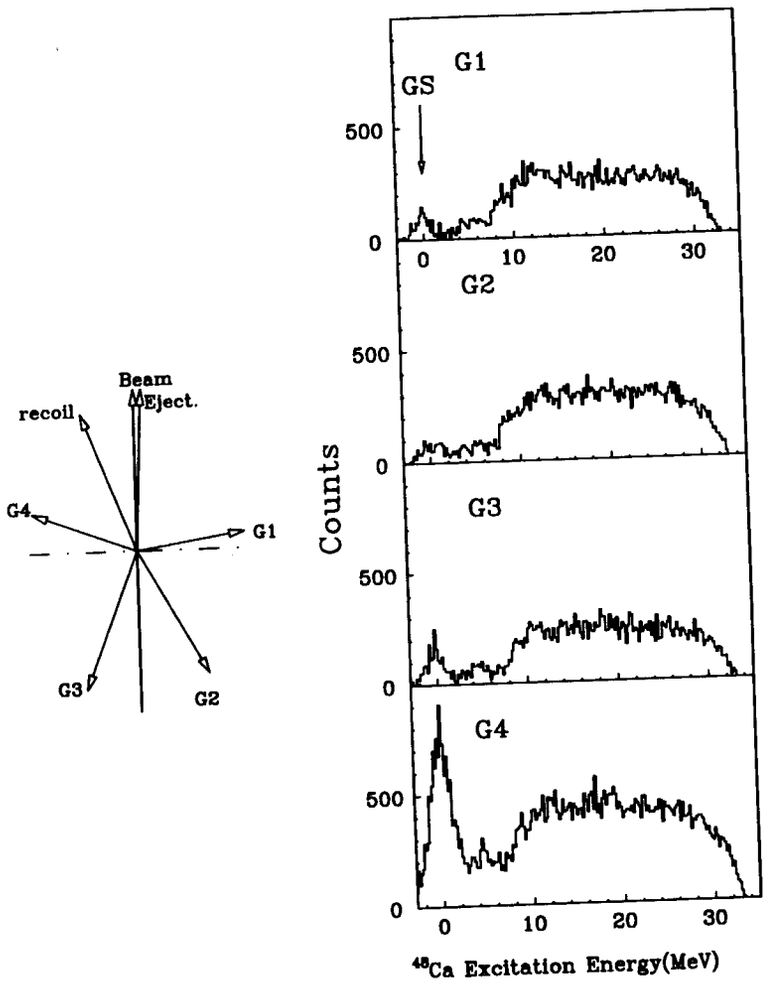
Beam
Eject.
recoil
G4
G1
G3
G2
G1
GS
G2
G3
G4
Counts
500
0
0
10
20
30
^{48}Ca Excitation Energy(MeV)

Fig 8

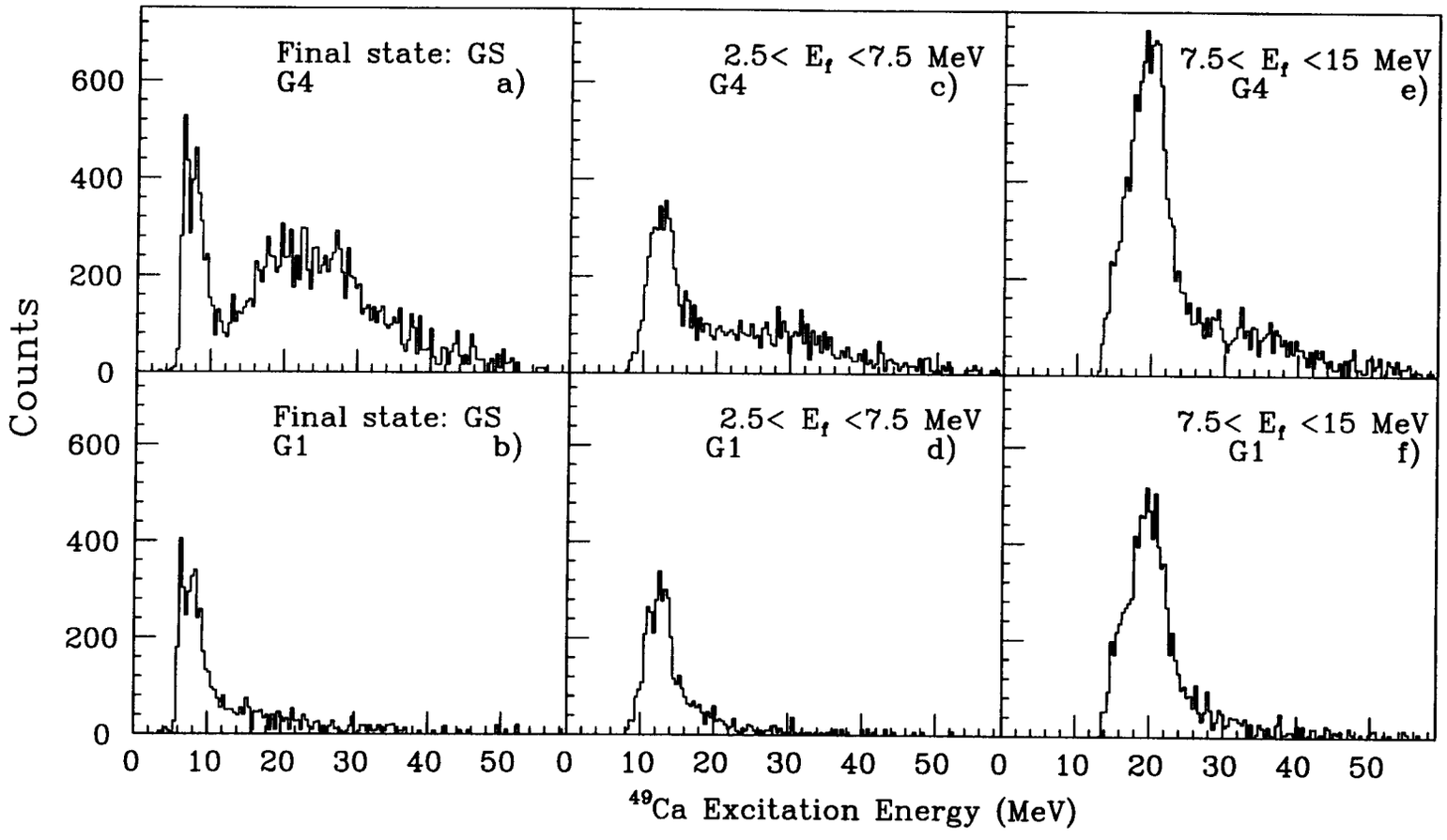
Final state: GS
G4
a)
2.5< E_f <7.5 MeV
G4
c)
7.5< E_f <15 MeV
G4
e)
Final state: GS
G1
b)
2.5< E_f <7.5 MeV
G1
d)
7.5< E_f <15 MeV
G1
f)
Counts
0
200
400
600
0 10 20 30 40 50
^{49}Ca Excitation Energy (MeV)

Fig. 9

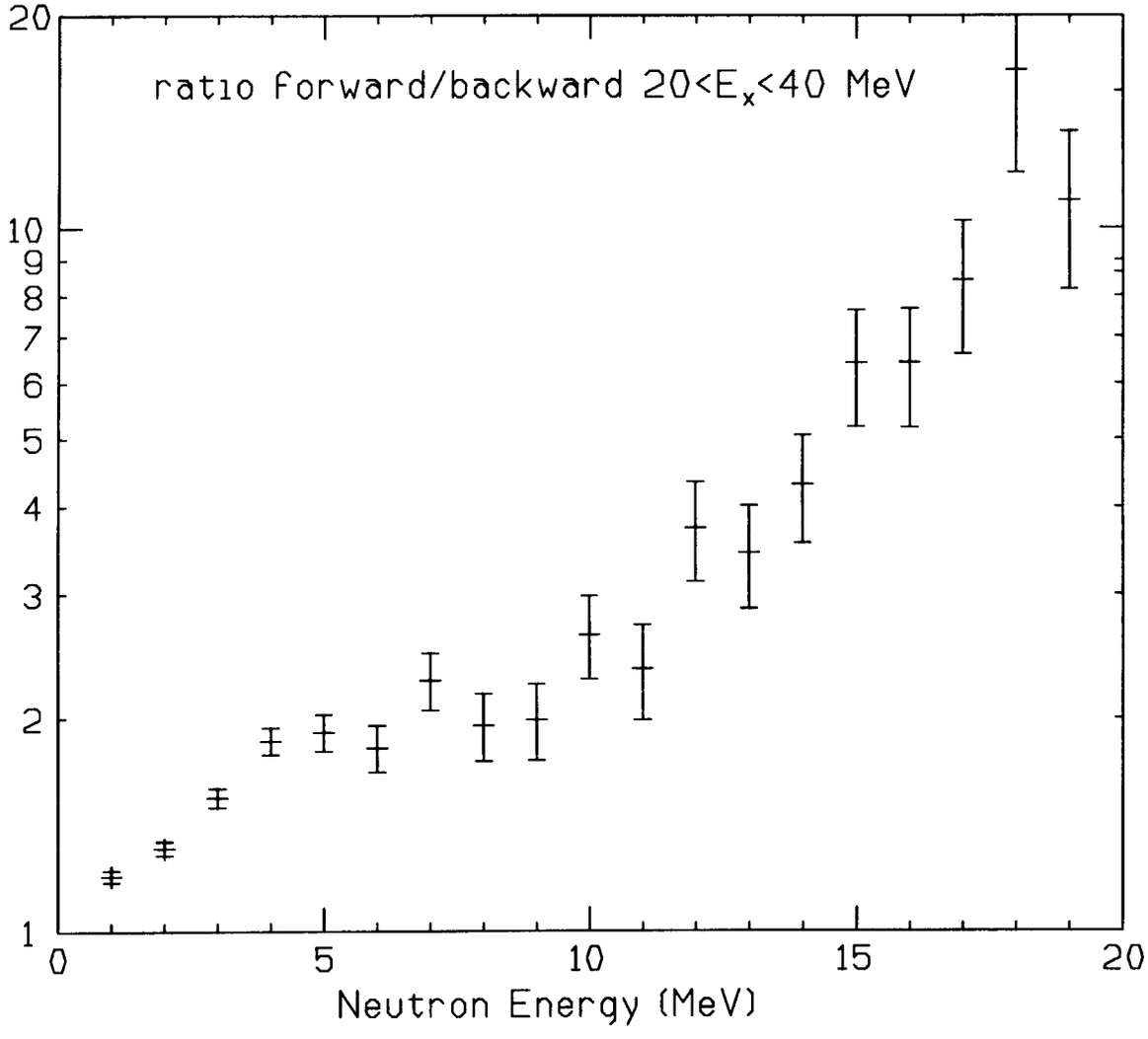
ratio forward/backward 20<E$_x$<40 MeV
20
10
9
8
7
6
5
4
3
2
1
0
5
10
15
20
Neutron Energy (MeV)

Fig 10

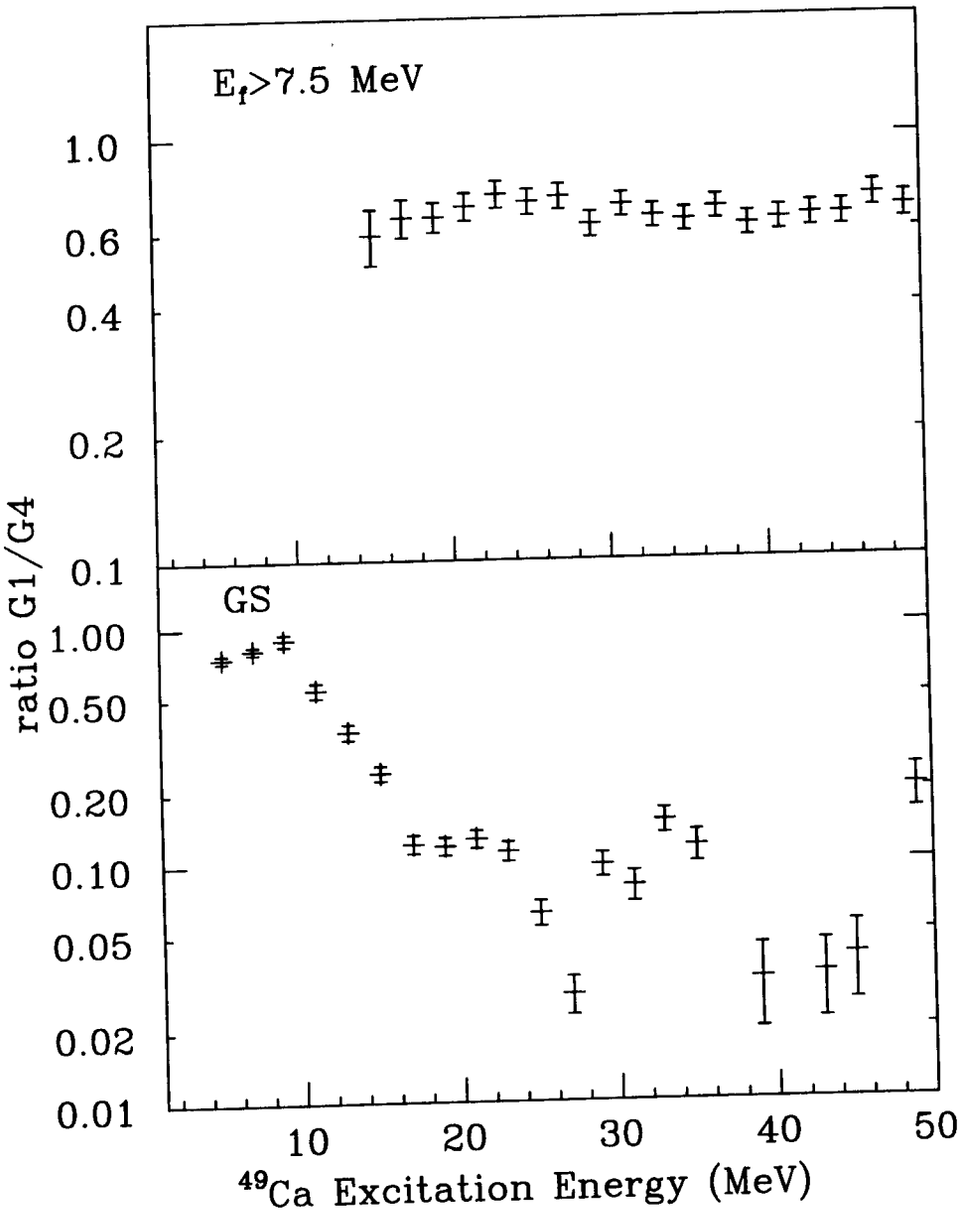
E_f>7.5 MeV
GS
ratio G1/G4
1.0
0.6
0.4
0.2
0.1
1.00
0.50
0.20
0.10
0.05
0.02
0.01
10
20
30
40
50
^{49}Ca Excitation Energy (MeV)

Fig 11

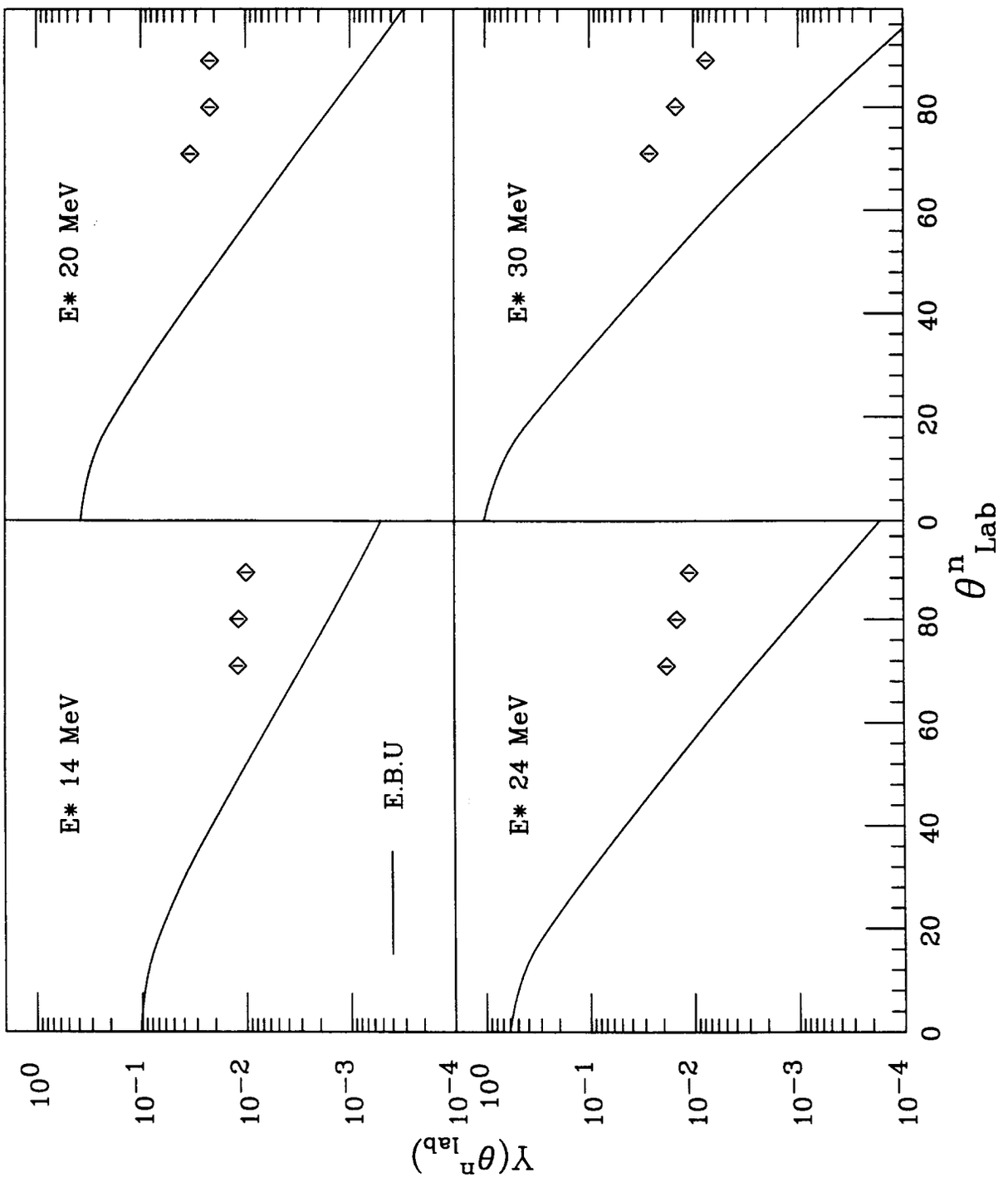
E* 14 MeV
E* 20 MeV
E* 24 MeV
E* 30 MeV
E.B.U
$Y(\theta^n_{lab})$
θ^n_{Lab}
10^0
10^{-1}
10^{-2}
10^{-3}
10^{-4}
0
20
40
60
80

Fig 12

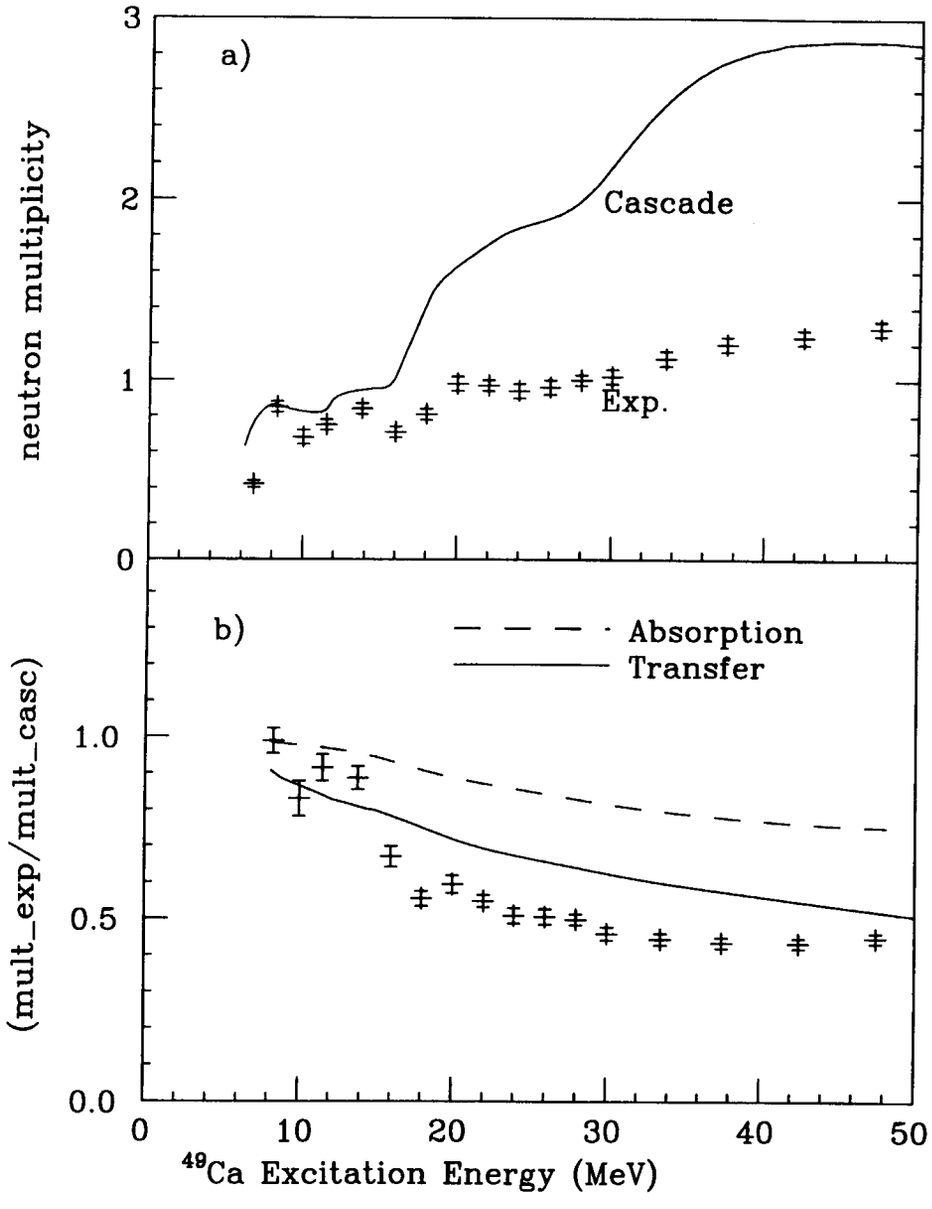
a)
Cascade
Exp.
neutron multiplicity
b)
Absorption
Transfer
(mult_exp/mult_casc)
^{49}Ca Excitation Energy (MeV)